Control of Domain Orientation in Block Copolymer Electrolyte Membranes at the Interface with Humid Air

By *Moon Jeong Park, Suhan Kim, Andrew M. Minor, Alexander Hexemer,* and *Nitash P. Balsara**

Ion-containing polymer electrolyte membranes (PEMs) have attracted considerable attention for their potential use in batteries and fuel cells.[1–5] Fuel cells are of particular interest due to their ability to produce power without degrading the environment.[6,7] Both random copolymers in which ion-containing groups are connected randomly to hydrophobic backbones[8–10] and block copolymers[3,5,11–16] in which ion-containing hydrophilic groups are sequestered in a fraction of the chains have been considered as PEMs. Block copolymer-based PEMs are ideally suited for fundamental studies, due to the fact that the size and shape of the ion-conducting channels are defined by the molecular structure of the copolymer and the water content.[3,5,12,14] This, in turn, enables optimization of PEMs for practical applications. In contrast, pathways for ion transport in random copolymer-based PEMs do not have a well-defined shape and size due to the polydisperse nature of the ionic domains.

While the effect of bulk morphology, degree of order, and water uptake on the conductivity of PEMs have been studied by several groups,[5,12,15,16] there is relatively little knowledge of the organization of the hydrophilic and hydrophobic domains at surfaces.[17] In dry air, the hydrophobic domains are expected to cover the air/PEM interface, due to lower surface tension of hydrophobic moieties. This may have a detrimental effect on the performance of the PEM, because hydration of the membrane, which is necessary for proton transport, requires penetration of the water molecules from the air into the membrane. The barriers to water penetration may be thermodynamic or kinetic in origin. One might expect that the PEM surface will become increasingly hydrophilic as the relative humidity (RH) of the air increases, but there are no quantitative studies of this effect. Predicting this is challenging, due to the fact that thermodynamic equilibrium is influenced by factors other than surface tension of the dry domains, such as chain connectivity, entropy, and domain geometry.

In this paper, we explore the orientation of domains in PEMs made from poly(styrenesulfonate-*b*-methylbutylene) copolymers (PSS-PMB) in contact with humid air. This paper is part of a series on the properties of PEMs made from PSS-PMB copolymers.[5,14] Our previous papers were concerned with bulk behavior. Here, we use atomic force microscopy (AFM) to explore surface topology, and grazing-incidence small-angle x-ray scattering (GISAXS), transmission electron microscopy (TEM) with focused ion beam (FIB), and electron microtomography to determine the domain orientation within the film. We demonstrate that at fixed composition, the sulfonation levels of the PSS-PMB copolymers play an important role in determining domain orientation. To our knowledge, this is the first study of the effect of the sulfonation level on domain orientation of PEMs in contact with humid air.

Our studies are related to the ''solvent-annealing'' process for controlling domain orientation in block copolymer films.[18,19] In these experiments, block copolymer films are exposed to solvent vapors and the effect of this exposure on domain orientation is observed. A polymer system that has been studied extensively are poly(ethylene oxide-*b*-styrene) (PEO-PS) diblock copolymers[20,21] sealed in a chamber containing an open jar of the solvent of interest, which can be either an organic solvent or water. It should be noted that the composition and temperature of the surrounding air in most solvent-annealing studies is not actively controlled. In contrast, the water content and temperature of the air surrounding our membranes is actively controlled throughout the annealing process.

We studied two PSS-PMB samples, with 25 and 49 mol% of the PS moieties sulfonated, referred to as P9(25) and P9(49), respectively, where 9 refers to the nominal molecular weight of the PS block of the parent copolymer in kg mol^{-1}. Our synthesis and characterization methods are described elsewhere.[14] Both P9(25) and P9(49) show hexagonally packed cylinder (HEX) morphologies, with hydrophobic PMB cylinders dispersed in a hydrophilic PSS matrix (Supporting Information). Increasing the sulfonation level from 25 to 49 mol% results in a slight increase in domain size, d, from 22 nm to 23 nm (d is the average spacing between (100) planes of HEX domains).

[*] Dr. M. J. Park, Prof. N. P. Balsara
Department of Chemical Engineering, University of California
Berkeley and Materials Sciences Division
Environmental Energy Technologies Division
Lawrence Berkeley National Laboratory
Berkeley, CA 94720 (USA)
E-mail: nbalsara@berkeley.edu
Dr. S. Kim, Prof. A. Minor
Department of Materials Sciences and Engineering
University of California
Berkeley and
National Center for Electron Microscopy
Lawrence Berkeley National Laboratory
Berkeley, CA 94720 (USA)
Dr. A. Hexemer
Advanced Light Source
University of California, Berkeley
Lawrence Berkeley National Laboratory
Berkeley, CA 94720 (USA)

DOI: 10.1002/adma.200801613

180 nm thick P9(25) films on Si wafers with native oxide layers were prepared by spin-coating from 4 wt% tetrahydrofuran (THF) solutions. The films were dried under vacuum for 5 days at 21 °C to remove residual solvent. The surface morphology of dried films, examined by AFM in tapping mode, is shown in Figure 1a. We found a coexistence of vertically oriented cylinders with limited long-range order and regions that appear disordered. The surface morphology of P9(25) is not affected by exposing to laboratory air (21 °C and RH = 32%), due to the negligible water uptake.[5] The morphology in Figure 1a thus represents that of the dry P9(25) films.

The films were then annealed in an oven in which both the temperature and humidity of the surrounding air were controlled. The characterization was performed in ex situ experiments after the films were removed from the oven. Based on the color changes of thin films from black (hydrated) to purple (dry), we conclude that the films dry within a few seconds after removal from the oven. We expect that this results in trapping of the hydrated morphology due to the rapid vitrification of the PSS chains. Previous studies have shown that equilibrium morphologies of copolymers with glassy blocks can be trapped by rapid vitrification.[22,23] In contrast, it is difficult to preserve the equilibrium morphology of semicrystalline materials such as Nafion and polyethylene.[24,25]

The surface morphology obtained after exposition of the 180 nm thick P9(25) film to saturated water vapor, RH = 98%, for 4 h at $T = 40$ °C is shown in Figure 1b. We see enhanced long-range order in the perpendicularly aligned cylinders, and a reduction of the disordered morphology. Further exposure to humid air for 24 h resulted in a highly ordered array of perpendicular cylinders, as shown in Figure 1c, and no evidence of disordered morphology. To establish the high degree of lateral ordering, an AFM image obtained from a 2 μm × 2 μm area is shown in Figure 1d. It is evident that the presence of moisture leads to a reduction in defect density, presumably due to the enhanced mobility of the hydrated PSS-PMB chains.

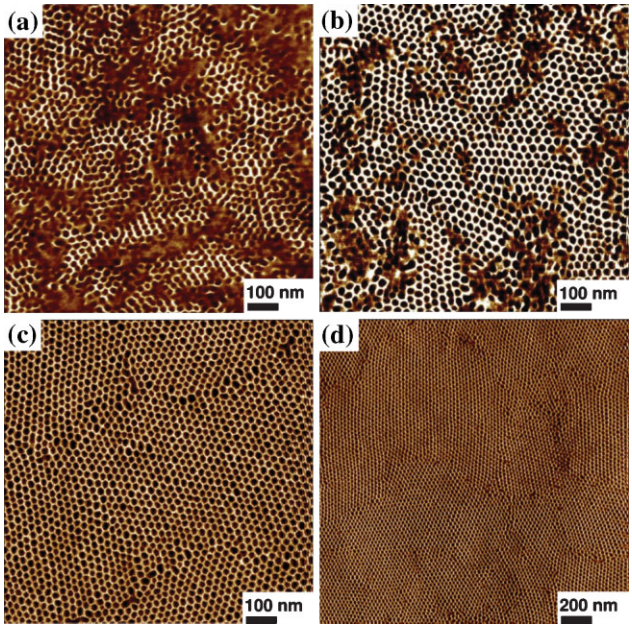

Figure 1. Surface morphologies of 180 nm thick P9(25) thin film a) as-cast, b) after exposure to humid air, RH = 98% and $T = 40$ °C, for 4 h, and c,d) after exposure to humid air, RH = 98% and $T = 40$ °C, for 24 h. a–c) 1 μm × 1 μm AFM phase images. d) 2 μm × 2 μm AFM phase image shows extent of lateral ordering in sample.

The fact that the hydrophilic matrix did not cover up the P9(25)/humid air interface is, perhaps, surprising. In dry air (RH = 0%), the surface tensions of the PSS and PMB phases of P9(25) are approximately 47 and 30 dyne/cm, respectively.[26] When the sample is exposed to humid air, water with surface tension of 72 dyne/cm selectively solvates the PSS domains. Bulk water uptake measurements under $T = 40$ °C and RH = 98% indicate that the weight fraction of water in the polymer is 24 wt %. We thus expect that the difference between the surface tensions of hydrated PSS and PMB domains substantially increase when the film is contacted with humid air. It has been argued in the literature that perpendicular orientations of block copolymer domains occur when the surface tensions of the domains are matched.[20,21] Our results indicate that other factors dominate the orientation of PSS-PMB copolymer domains at the polymer/humid air interface. Our arguments thus far have ignored the change in surface tension of the microphases due to the presence of humidity, which, to our knowledge, has neither been measured nor estimated.

Optical microscopy and AFM revealed no detectable dewetting of the P9(25) films at RH = 98% and $T = 40$ °C up to 80 h. On the contrary, exposing the P9(25) sample to humid air leads to a reduction in root mean square (RMS) surface roughness from 5 to 2 nm (see Supporting Information). When P9(25) was exposed to humid air (RH = 98%) at $T = 50$ °C, hole and island structures were observed, and the film dewetted after 1 h of exposure.

Next we study the morphology of the P9(25) film beneath the surface in position space. The standard technique of delaminating polymer films using an epoxy matrix followed by microtoming was not used in the present study, because of the deformation of surface morphology at both silicon and air during sample preparation. This is due, in part, to the strong bonds between the SO_3H groups and SiO_2. Typical images obtained by this method are shown in the Supporting Information. We thus used a shadow-FIB technique for studying the subsurface structure of our films. The film was first stained with ruthenium tetroxide (RuO_4) and placed in the FIB chamber facing down, away from the ion beam to avoid direct exposure. A low-dose (10 pA) Ga^{2+} ion beam is positioned at the corner of the sample and normal to the film. The sample is then etched up to the location of interest. Typically, two such etching steps were used to obtain an electron-beam transmittable slice of the sample. The shadow-FIB method does not require a protective Pt layer sputtered on the top surface of the sample, as is necessary in the lift-out FIB method.[23,27] This helps to avoid any potential damage to the polymer/air interface caused by metal deposition.[28] Figure 2a shows the shadow FIB-TEM image of the as-cast P9(25) film that was only contacted with dry air. Perpendicularly oriented cylinders are seen in a small region near the air interface (top left in Fig. 2a). However, most of the sample is poorly ordered. Exposure to air with RH = 98% and $T = 40$ °C for 24 h results in a dramatic change in the cross-sectional structure, as shown in Figure 2b. The dark band at the air surface is a RuO_4 layer deposited during staining. Beneath the RuO_4 band, perpendi-

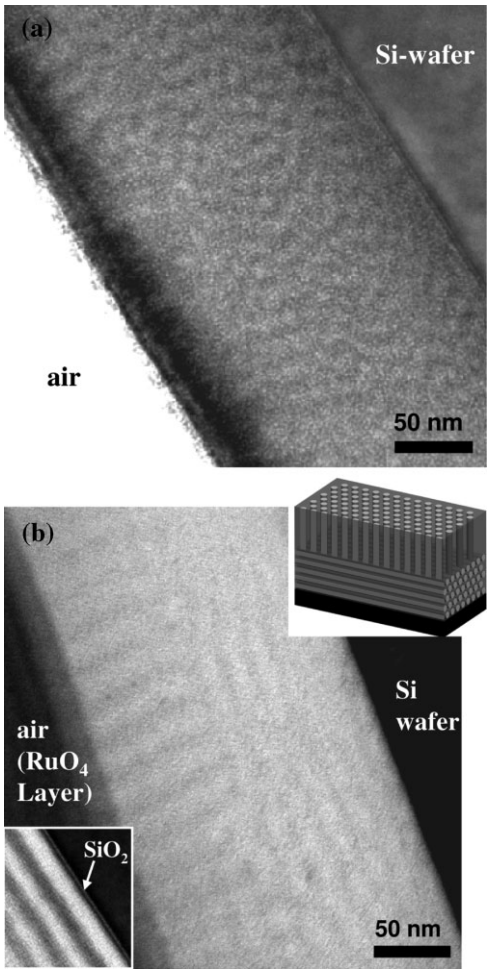

Figure 2. Cross-sectional shadow FIB-TEM images of P9(25) film a) as-cast and b) after exposure to humid air, RH = 98% and $T = 40\,^{\circ}C$, for 24 h. b) Coexisting perpendicular and parallel orientations of cylinders propagating from the air surface and Si-wafer, respectively. A schematic illustration of this is shown in inset in b). The higher-magnification TEM image shown in the bottom left inset in b) indicates the presence of native SiO_2 layers (bright) and preferential wetting of PSS (dark) on substrate. The PSS domain was darkened by RuO_4 staining.

cular cylinders are seen to propagate from the top to the center of the film. The cylinders near the Si surface are oriented parallel to the plane of the film, and this morphology propagates through the bottom half of the film. A schematic of the film morphology is shown in the inset in Figure 2b. The location of the grain boundary in the middle of the film suggests that the driving forces orienting the cylinders induced by silicon and humid air are comparable in magnitude. The diameters of the cylinders at the air surface appear to be larger than those at the Si substrate. Since the time required for the water to penetrate the film is much less than 2 h,[13] the difference between the domain sizes in the two orientations must be due to differences in chain stretching in parallel and perpendicular domains. To our knowledge, Figure 2a and b represent the first cross-sectional shadow-FIB-TEM images of microphase-separated polymers.

The bottom left inset box of Figure 2b is a high-resolution TEM image of the morphology in the proximity of the SiO_2 surface, which appears as a bright stripe in the image. We see the presence of a thin dark layer of PSS covering the polymer/SiO_2 interface, which is attributed to the attractive interactions between SO_3H groups and the SiO_2. Knowledge of the presence or absence of such a layer would be crucial at the PEM/catalyst interface, due to the need for proton transport at the interface.

Figure 3a and b show the GISAXS intensity as a function of q_y and q_z, the scattering vectors along the horizontal and vertical directions, respectively (ignoring the shallow angle of grazing incidence), of the P9(25) film after exposure to RH = 98% and $T = 40\,^{\circ}C$ air for 24 h measured at different incident angles (α_i). When α_i is below the critical angle of the polymer film (α_c),

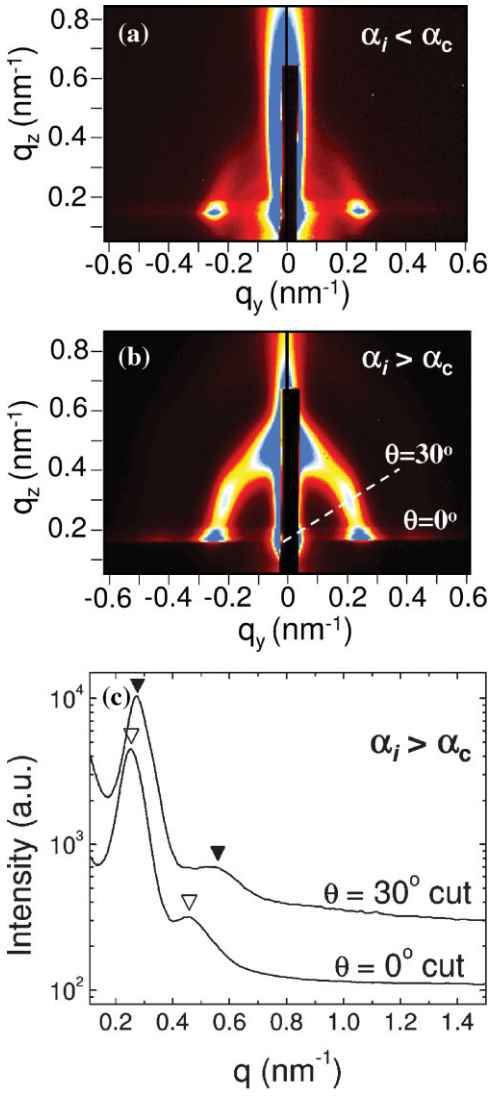

Figure 3. GISAXS patterns of 180 nm thick P9(25) film after exposure to humid air with RH = 98% and $T = 40\,^{\circ}C$, for 24 h: a) $\alpha_i = 0.14^{\circ}$ (below α_c) and b) $\alpha_i = 0.21^{\circ}$ (above α_c) were used to determine the domain orientation near the air surface and through the entire film thickness, respectively. c) Sector-averaged GISAXS profiles of P9(25) thin film measured at $\alpha_i = 0.21^{\circ}$. Bragg peaks at q^*,$\sqrt{3}q^*$ ($\triangledown$, $\theta = 0^{\circ}$), and at q^*, $2q^*$ ($\blacktriangledown$, $\theta = 30^{\circ}$) are shown. The sector-averaged GISAXS profile at $\theta = 30^{\circ}$ is offset vertically by a factor of 5 for clarity.

information on the orientation is obtained from the upper part of the film only, whereas for angles larger than α_c, the scattering pattern contains information about the entire film.[29] For PSS-PMB, α_c was determined to be 0.16 °. The GISAXS pattern obtained at $\alpha_i = 0.14$ ° (Fig. 3a), which is below the α_c, shows 2 spots centered at $q_y = 0.25$ nm^{-1} at constant $q_z = \pm 0.15$ nm^{-1}, i.e., at the angle of specular reflection, with high-order peaks at 1:$\sqrt{3}$ ratio. This pattern indicates the presence of HEX domains in the perpendicular orientation in the vicinity of the air surface.[30] The GISAXS pattern obtained at $\alpha_i = 0.21$ ° (Fig. 3b), which is above the α_c, contains two strong spots at the azimuthal angles (θ) of 30 ° and 150 °, with high-order peaks at 1:2 ratio. This can be attributed to the dominant (100) orientation of HEX structures along the Si-substrate.[29] The scattering ring seen in Figure 3b is attributed to the mixed orientations present at the junction between parallel and perpendicular orientations. The GISAXS data confirm the film morphology proposed based on AFM and shadow FIB-TEM. Figure 3c shows the sector-averaged GISAXS intensity along $\theta = 0$ °and $\theta = 30$ ° (±5 °) for $\alpha_i = 0.21$ °. The $\theta = 0$ ° data contain peaks at q^* and $\sqrt{3}q^*$ (perpendicular orientation), while the data at $\theta = 30$°contain peaks at q^* and $2q^*$ (parallel orientation), where $q^* = 2\pi/d$. It is clear from Figure 3c that q^* corresponding to the perpendicular orientation is lower than that corresponding to the parallel orientation, in good agreement with the shadow FIB-TEM data in Figure 2b. The calculated d was 25 nm for the perpendicular cylinders near the air surface, and 23 nm for the parallel cylinders near the Si-substrate.

To study the effect of sulfonation levels on domain orientation, a 250 nm thick P9(49) film was prepared on a Si-wafer by the same procedure as that used to prepare the P9(25) film. Figure 4a shows a typical AFM image obtained from the as-cast film. We see no evidence of microphase separation on the P9(49) surface, contrary to the P9(25) film. The lack of order on top of the P9(49) film is undoubtedly a non-equilibrium effect. As sulfonation increases, THF, the solvent used in spin casting, becomes an increasingly poor solvent for the PSS phase. It is conceivable that micelle formation in solution leads to the disordered morphology seen in Figure 4a. Figure 4b shows the effect of exposure of the P9(49) film to saturated air with RH = 98%, at $T = 25$ °C for 4 h. Parallel cylinders are observed over the entire free surface of the sample. This is the opposite of what was observed in P9(25), where exposure to humid air led to perpendicular cylinders. Since water concentration in P9(49) is 38 wt%,[5] it is evident that the concomitant increase in the amount of water in the PSS phase is enough to suppress the exposure of the hydrophobic PMB domains at the humid air interface. The large water concentration in P9(49) leads to plasticization of the PSS chains, and thus the time to complete lateral ordering is much shorter than P9(25) sample. In addition, the temperature at which ordering is observed is lower than that needed to obtain surface ordering in P9(25). Exposing the P9(49) film to humid air at 40 °C leads to dewetting within 0.5 h.

In Figure 4c and d, we show cross-sectional shadow-FIB-TEM images of dry and humidified versions of P9(49), respectively. As shown in Figure 4c, the top of the as-cast dry film is devoid of long-range order, in good agreement with the AFM result (Fig. 4a). Parallel cylinders are observed near the Si-substrate, with a considerably higher degree of ordering than P9(25). This is

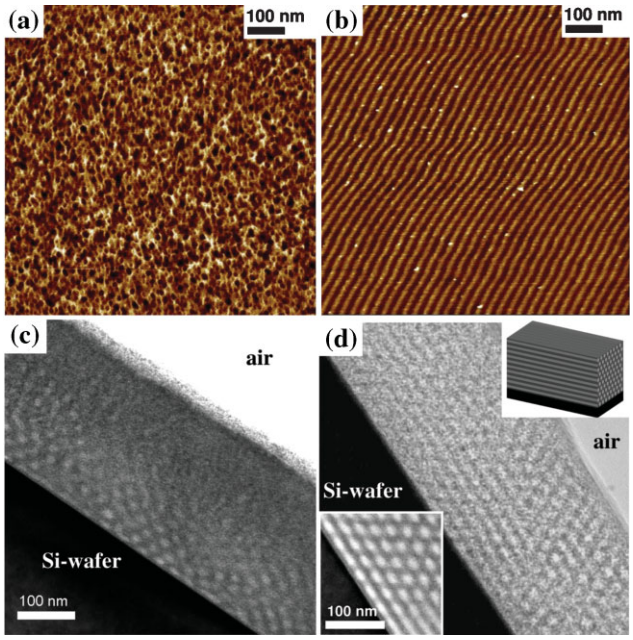

Figure 4. Surface morphologies of P9(49) films a) as-cast and b) after exposure to humid air with RH = 98% and $T = 25$ °C, for 4 h (1 μm × 1 μm, AFM phase images). Morphology through the film by cross-sectional shadow FIB-TEM, for film c) as-cast and d) after exposure to humid air with RH = 98% and $T = 25$ °C, for 4 h. The TEM image in d) clearly shows the dominant parallel orientation of cylinders propagating from both the air and the Si-wafer interfaces. A schematic illustration of the film structure is shown in inset in d). The higher-magnification TEM image, shown in the bottom left inset in d), indicates the preferential wetting of PSS (dark) on substrate. The PSS domain was darkened by RuO_4 staining.

presumably due to the stronger interactions between the SiO_2 layer and the PSS chains in P9(49) relative to P9(25). We expect the exposure of P9(49) to humid air to result in parallel cylinders throughout the sample, because this is the preferred orientation at both surfaces. The shadow FIB-TEM data in Figure 4d, obtained after exposure to air with RH = 98% at 25 °C, confirm this result. The left bottom inset box of Figure 4d, obtained with high-resolution shadow FIB-TEM, confirms selective wetting of the substrate by PSS. In this respect, P9(25) and P9(49) are similar. The d of the P9(49) sample increased from 23 nm to 26 nm upon humidification, implying that significant swelling occurred during the exposure of the sample to humid air.

We conclude by examining domain orientation in free-standing PSS-PMB films. This enables determination of the effect of humid air on domain orientation without interference from the Si substrate. 200 nm thick P9(25) films were prepared by cryogenic microtoming, transferred onto a Cu grid, exposed to air with RH = 98%, at $T = 40$ °C for 24 h, dried in the laboratory air for 12 h, and stained with RuO_4. The conventional 2D TEM image of the top view of the free-standing film, shown in Figure 5a, indicates the presence of perpendicular cylinders. The morphology within the film was determined by electron microtomography. Fifty-three TEM images were obtained using tilt angles ranging from −52 ° to +52 °. Alignment of the images was carried out with the aid of 10 nm Au nanoparticles (dark spots in Fig. 5a), which were deposited on top of formvar-coated Cu grids

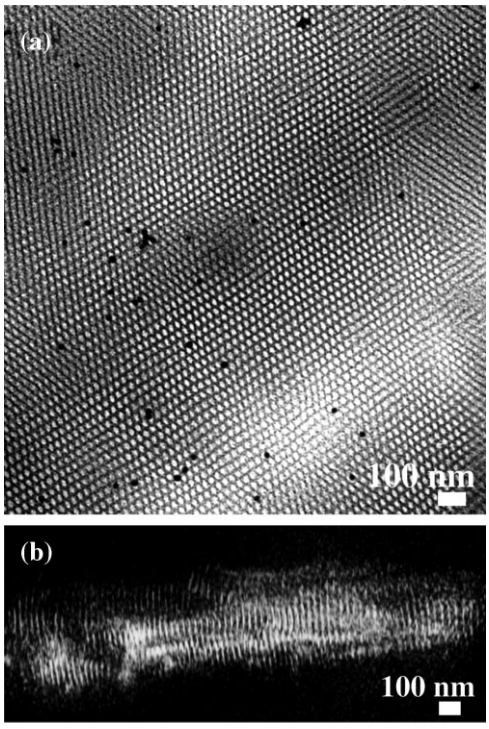

Figure 5. a) TEM image of a 200 nm thick P9(25) free-standing film after exposure to air with RH = 98%, $T = 40\,^{\circ}C$ for 24 h. b) 3D electron microtomography image obtained from 53 tilt-series images of the sample in a). The PSS domain was darkened by RuO_4 staining.

before microtoming. The reconstructed 3D structure obtained using techniques described in refs. [31,32] is shown in Figure 5b. Vertically oriented cylinders are seen spanning the entire thickness of the free-standing P9(25) film when both surfaces of the sample are exposed to humid air.

In summary, we have demonstrated that the alignment of domains of PSS-PMB PEMs at the polymer/humid air interface depends crucially on the sulfonation level of the PSS block. The presence of hydrophilic microphases does not, by itself, guarantee the absence of hydrophobic domains at the humid air surface. In particular, we have shown that the hydrophobic PMB cylinders in sample P9(25) are oriented perpendicular to the plane of the film, and they are thus in contact with humid air at equilibrium. In contrast, the PMB cylinders in sample P9(49) are oriented parallel to the plane of the film, and are buried beneath the hydrophilic PSS matrix. It is important to note that these qualitative differences are obtained in spite of the fact that there is virtually no difference in the bulk morphology of P9(25) and P9(49). The kind of information that we have obtained here is crucial for using PEMs in applications such as fuel cells and water purification, because it demonstrates that pathways for proton and water diffusion may be cut-off at the surfaces due to the interplay between surface tension, chain connectivity, and the balance between hydrophilicity and hydrophobicity of the membrane. Further studies of the effect of block copolymer molecular weight and composition, and the chemical composition of the substrate (e.g., platinum, which is used as a catalyst in fuel cells) seem warranted.

Experimental

Materials: PS-PMB with PS and PMB molecular weights of 9.1 and 8.7 kg mol^{-1}, respectively, was synthesized by sequential anionic polymerization of styrene and isoprene followed by selective hydrogenation of polydiene. The polydispersity index of the copolymer was 1.02. The PS block was partially sulfonated, and the resulting copolymer is referred to as PSS-PMB. Details concerning the synthesis procedures used are given in our recent publications [14].

Thin-Film Preparation and Characterization: 4 wt % solutions of PSS-PMB in THF were spin-coated on a Si wafer with a native oxide layer. The films were dried in a vacuum oven for 5 days at 21 °C and then placed inside an ESPEC SH-241 humidity-controlled oven to expose the samples to the specified humidities and temperatures. A variable-angle multi-wavelength ellipsometer was used to measure the thickness of the films. Surface morphology was determined using AFM (Digital Instruments, Nanoscope III) in tapping mode. All measurements were performed with a phase contrast value of 10°. GISAXS measurements were carried out at the beamline 7.3.3 equipped with a charge-coupled device detector (2304 × 2304 pixels) at the Advanced Light Source (ALS), Lawrence Berkeley National Laboratory (LBNL). The sample-to-detector distance was 2.28 m, and the incident angle was varied from 0.10° to 0.21° in 0.01° increments.

FIB Etching and Cross-Sectional TEM: Samples for TEM studies were also prepared by spin-coating. Selective staining of PSS domains was accomplished by exposure to RuO_4 vapor for 2 h. Cross-sectional TEM samples were then prepared by shadow-FIB technique using a FEI Strata 235 Dual Beam FIB system operated at 30 kV. Etching was performed with a 10 pA Ga^{2+} ion beam. Imaging of etched samples was performed using a JEOL 3010 microscope operated at 300 kV.

Characterization of Bulk PSS-PMB Samples: Free-standing PSS-PMB TEM samples were prepared by cryo-microtoming at −100 °C to yield sections with thicknesses in the 80–200 nm range, using an RMC Boeckeler PT XL Ultramicrotome. Electron microscopy images of samples stained with RuO_4 vapor were obtained using a Philips CM300/FEG microscope operated at 300 kV equipped with double-tilt sample holder.

Acknowledgements

Major funding for this work was provided through the Electron Microscopy of Soft Matter Program at LBNL supported by the Director, Office of Science, Office of Basic Energy Sciences, Materials Sciences and Engineering Division, of the U.S. Department of Energy under Contract No. DE-AC02-05CH11231. This work was supported by the Assistant Secretary for Energy Efficiency and Renewable Energy, Office of Hydrogen, Fuel Cells and Infrastructure Technologies of the U.S. Department of Energy under Contract No. DE-AC02-05CH11231. TEM was performed at the National Center for Electron Microscopy at LBNL. GISAXS measurements were conducted on the beam line 7.3.3 instrument at the ALS (LBNL). We gratefully acknowledge Prof. Rachel Segalman for providing access to the AFM. Supporting Information is available online from Wiley InterScience or from the authors.

Received: June 12, 2008
Revised: July 31, 2008

[1] P. P. Soo, B. Y. Huang, Y. I. Jang, Y. M. Chiang, D. R. Sadoway, A. M. Mayes, *J. Electrochem. Soc.* **1999**, *146*, 32.
[2] B.-K. Cho, A. Jain, S. M. Gruner, U. Wiesner, *Science* **2004**, *305*, 1598.
[3] Y. A. Elabd, F. L. Beyer, C. W. Walker, *J. Membr. Sci.* **2004**, *231*, 181.
[4] M. Singh, O. Odusanya, G. M. Wilmes, H. B. Eitouni, E. D. Gomez, A. J. Patel, V. L. Chen, M. J. Park, P. Fragouli, H. Iatrou, N. Hadjichristidis, D. Cookson, N. P. Balsara, *Macromolecules* **2007**, *40*, 4578.

[5] M. J. Park, K. H. Downing, A. Jackson, E. D. Gomez, A. M. Minor, D. Cookson, A. Z. Weber, N. P. Balsara, *Nano Lett.* **2007**, *7*, 3547.

[6] K. D. Kreuer, in: *Handbook of Fuel Cell – Fundamentals, Technology and Applications*, Vol. *3*, Part 3 (Eds: W. Vielstich, A. Lamm, H. A. Gasteiger), Wiley, Chichester, UK **2003**.

[7] Y. Shao, G. Yin, Z. Wang, Y. Gao, *J. Power Sources* **2007**, *167*, 235.

[8] F. Wang, M. Hickner, Y. S. Kim, T. A. Zawodzinski, J. E. McGrath, *J. Membr. Sci.* **2002**, *197*, 231.

[9] J. F. Ding, C. Chuy, S. Holdcroft, *Adv. Funct. Mater.* **2002**, *12*, 389.

[10] R. W. Kopitzke, C. A. Linkous, H. R. Anderson, G. L. Nelson, *J. Electrochem. Soc.* **2000**, *147*, 1677.

[11] Z. Q. Shi, S. Holdcroft, *Macromolecules* **2005**, *38*, 4193.

[12] Y. A. Elabd, E. Napadensky, C. W. Walker, K. I. Winey, *Macromolecules* **2006**, *39*, 399.

[13] M. J. Park, A. Nedoma, P. L. Geissler, N. P. Balsara, A. Jackson, D. Cookson, *Macromolecules* **2008**, *41*, 2271.

[14] M. J. Park, N. P. Balsara, *Macromolecules* **2008**, *41*, 3678.

[15] J. Kim, B. Kim, B. Jung, Y. S. Kang, H. Y. Ha, I.-H. Oh, K. J. Ihn, *Macromol. Rapid Commun.* **2002**, *23*, 753.

[16] J. Won, H. H. Park, Y. J. Kim, S. W. Choi, H. Y. Ha, I.-H. Oh, H. S. Kim, Y. S. Kang, K. J. Jin, *Macromolecules* **2003**, *36*, 3228.

[17] D. A. Bussian, J. R. O'Dea, H. Metiu, S. K. Buratto, *Nano Lett.* **2007**, *7*, 227.

[18] G. Kim, M. Libera, *Macromolecules* **1998**, *31*, 2569.

[19] S. Ludwigs, A. Böker, A. Voronov, N. Rehse, R. Magerle, G. Krausch, *Nat. Mater.* **2003**, *2*, 744.

[20] Z. Lin, D. H. Kim, X. Wu, L. Boosahda, D. Stone, L. LaRose, T. P. Russell, *Adv. Mater.* **2002**, *14*, 1373.

[21] S. H. Kim, M. J. Misner, T. Xu, M. Kimura, T. P. Russell, *Adv. Mater.* **2003**, *15*, 226.

[22] L. Zhu, S. Z. D. Cheng, B. H. Calhoun, Q. Ge, R. P. Quirk, E. L. Thomas, B. S. Hsiao, F. Yeh, B. Lotz, *Polymer* **2001**, *42*, 5829.

[23] J. Bang, B. J. Kim, G. E. Stein, T. P. Russell, X. Li, J. Wang, E. J. Kramer, C. J. Hawker, *Macromolecules* **2007**, *40*, 7019.

[24] M.-H. Kim, C. J. Glinka, S. A. Grot, W. G. Grot, *Macromolecules* **2006**, *39*, 4775.

[25] Y.-L. Loo, R. A. Register, A. J. Ryan, *Macromolecules* **2002**, *35*, 2365.

[26] J. Brandrup, E. H. Immergut, E. A. Grulke, A. Abe, D. R. Bloch, in *Polymer Handbook*, 4th Ed., John Wiley and Sons, New York **1999**.

[27] H. Whitea, Y. Pua, M. Rafailovicha, J. Sokolova, A. H. Kingb, L. A. Giannuzzic, C. Urbanik-Shannonc, B. W. Kempshallc, A. Eisenbergd, S. A. Schwarze, Y. M. Strzhemechnye, *Polymer* **2001**, *42*, 1613.

[28] S. Welz, N. Browning, A. M. Minor, *Microsc. Microanal.* **2005**, *11*, 834.

[29] B. Lee, I. Park, J. Yoon, S. Park, J. Kim, K. W. Kim, T. Chang, M. Ree, *Macromolecules* **2005**, *38*, 4311.

[30] V. Khanna, E. W. Cochran, A. Hexamer, G. E. Stein, G. H. Fredrickson, E. J. Kramer, X. Li, J. Wang, S. F. Hahn, *Macromolecules* **2006**, *39*, 9346.

[31] K. H. Downing, H. Meisheng, H.-R. Wenk, M. A. O'Keefe, *Nature* **1990**, *348*, 525.

[32] R. J. Spontak, J. C. Fung, M. B. Braunfeld, J. W. Sedat, D. A. Agard, L. Kane, S. D. Smith, M. M. Satkowski, A. Ashraf, D. A. Hajduk, S. M. Gruner, *Macromolecules* **1996**, *29*, 4494.